Precipitation Observed in Oklahoma Mesoscale Convective Systems with a Polarimetric Radar

A. V. RYZHKOV* AND D. S. ZRNIĆ

NOAA/ERL, National Severe Storms Laboratory, Norman, Oklahoma

(Manuscript received 18 February 1993, in final form 14 September 1993)

ABSTRACT

In this paper, the fields of three radar polarimetric variables—differential reflectivity Z_{DR}, specific differential phase K_{DP}, and correlation coefficient between horizontally (H) and vertically (V) polarized echoes ρ_{hv}—along with radar reflectivity Z_h, are examined within two Oklahoma mesoscale convective systems (MCSs). The analysis of the whole set of polarimetric variables reveals at least three types of hydrometeor populations in the precipitation within these MCSs. It seems to be possible to discriminate between pure liquid raindrops, drops with ice cores inside them, and mixed-phase precipitation containing rain and hail using joint analysis of all the polarimetric measurands available. Hail-bearing zones are characterized by significant reduction of Z_{DR} and ρ_{hv}, as well as large values of Z_h. Specific differential phase K_{DP} is usually high in these zones, and sometimes a pronounced differential phase shift upon scattering is evident.

Experimental data show that the differential phase Φ_{DP} and its derivative K_{DP} are reliable indicators of liquid water in heavy precipitation. A negative bias of Z_{DR} due to differential attenuation in precipitation could be significant in this type of storm. The validity of the correction scheme for Z_{DR} estimates based on the Φ_{DP} evaluation proposed in earlier theoretical papers was examined. It was found that differential attenuation was underestimated at least twofold in the previous theoretical predictions.

1. Introduction

Polarimetric radar measurements provide a unique opportunity to analyze the microphysical properties and phase composition of hydrometeors within clouds and precipitation, as well as to distinguish between liquid and solid particles. One of the most important applications of polarization methods in radar meteorology is the recognition of hail regions within intense convective storms.

The majority of research polarimetric weather radars in the United States utilize switching between horizontal and vertical polarizations of the transmitted wave, and have one receiver to process the backscattered polarization signals. This type of polarizer can provide measurements of at least three polarization parameters: differential reflectivity Z_{DR}, correlation coefficient between horizontally (H) and vertically (V) polarized echoes ρ_{hv}, and differential phase shift Φ_{DP} between them. Specific differential phase or differential propagation constant K_{DP} is a range derivative of Φ_{DP}. All these polarization parameters can be used to discriminate between hail, rain, and mixed-phased precipitation.

Using linear polarization radar data, Leitao and Watson (1984) established a boundary in the Z_h–Z_{DR} plane, separating rain from hail.[1] They concluded that large values of radar reflectivity Z_h together with low values of Z_{DR} might be caused by tumbling hail within the resolution volume. Calculations by Aydin and Zhao (1990) and Aydin et al. (1991) showed that for large water-coated melting hailstones, Z_{DR} exhibits a complicated dependence on particle size, wavelength, and the thickness of the water shell.

Balakrishnan and Zrnić (1990a) suggested a technique for identification of precipitation type on the basis of joint analysis of Z_h, Z_{DR}, and K_{DP}. According to them, specific differential phase yields a good estimate of liquid water in a rain–hail mixture and is not sensitive to dry hail with small refractive index or randomly oriented hail particles. But as has been shown by Aydin and Zhao (1990), highly oriented melting hailstones could produce K_{DP} values that are significantly different from zero. There are two other useful applications of the differential phase measurements. One is the possibility to correct Z_{DR} estimates for differential attenuation effects using relations between K_{DP} and specific differential attenuation A_{DP}, which was

* Permanent affiliation: Main Geophysical Observatory, St. Petersburg, Russia.

Corresponding author address: Dr. A. V. Ryzhkov, NOAA/ERL/NSSL, 1313 Halley Circle, Norman, OK 73069.

[1] Henceforth Z_h will indicate the reflectivity factor for horizontally polarized waves.

derived theoretically by Bringi et al. (1990) and Jameson (1992). The Z_{DR} bias due to propagation effects could be significant in intense storms even at *S*-band frequencies. So far, this proposed technique has not been experimentally verified.

In general, Φ_{DP} consists of two parts: cumulative phase shift due to propagation through anisotropic media, and backscatter differential phase shift δ, indicating non-Rayleigh scattering effects. Nonzero values of δ at 10-cm wavelength are attributed to large hydrometeors with a high degree of common alignment.

The utility of the correlation coefficient $|\rho_{hv}(0)|$ (henceforth ρ_{hv}) for determining precipitation type and gauging hail size was examined by Balakrishnan and Zrnić (1990b). According to their model, pure rain and pure small hail are characterized by ρ_{hv} values close to unity. But for mixed-phase precipitation, lower correlation is expected because ρ_{hv} decreases as the variety of hydrometeor shapes and orientations increases. This occurs, for instance, in the melting layer where solid and liquid particles coexist. Well-pronounced minimum values of ρ_{hv} slightly below the melting level in stratiform precipitation were reported by many investigators (Illingworth and Caylor 1989; Balakrishnan and Zrnić 1990b). But up to now, there were very few experimental datasets concerning the correlation within strong hailstorms.

The main objective of this paper is to present a comprehensive analysis of measurements of the available polarization variables made within severe storms. Two Oklahoma mesoscale convective system (MCS) cases are examined. The emphasis of the analysis is on the interrelation between spatial distributions of radar reflectivity, differential reflectivity, specific differential phase, and correlation coefficient. Another goal is to verify experimentally the results of model calculations (Balakrishnan and Zrnić 1990a,b) concerning ρ_{hv} and K_{DP} in areas of mixed phase precipitation and to check the technique for correcting Z_{DR} biases caused by propagation effects through anisotropic media, as suggested by Bringi et al. (1990).

2. Radar description

Recent upgrades of the NSSL polarimetric Doppler radar (referred to as the Cimarron radar) (Zahrai and Zrnić 1993) created opportunities for the collection and comprehensive analysis of polarimetric data. Although a fast switch to alter the transmission of vertical and horizontal polarization was available before the upgrade (Carter et al. 1986), the capability to examine large spatial areas was restricted because the various polarimetric variables could not be computed in real time. All computations were done on recorded time series data (Sachidananda and Zrnić 1987; Balakrishnan and Zrnić 1990b); this required slow scans and resulted in limited range coverage. After May 1992, the polarimetric and Doppler variables became available in real time at all range locations (768, spaced by 1 μs); so large three-dimensional arrays of polarization measurands could be examined.

The Cimarron radar (wavelength 10 cm) is located approximately 40 km to the northwest of the NSSL's main facility in Norman, Oklahoma. The radar is operated by remote control via a 9600-baud telephone line. Real-time data are transmitted to the central facility by a microwave link. The main radar parameters are listed in Table 1.

Special data processing is implemented on the Cimarron radar to simultaneously obtain the spectral moments (reflectivity factor Z_h, mean Doppler velocity v, spectrum width σ_v) and the polarimetric variables (differential reflectivity Z_{DR}, differential phase Φ_{DP}, and correlation coefficient ρ_{hv}) in real time. The alternate polarization switching that enables estimation of polarization-dependent parameters affects the estimates of the first three Doppler spectral moments, so conventional algorithms were modified. It is possible to display and record in real-time six variables, Z_h, v, σ_v, Z_{DR}, Φ_{DP}, and ρ_{hv}, from the 768 consecutive range locations. The number of pairs for estimation of these variables is typically 128. Zahrai and Zrnić (1993) provide a detailed description of the radar and processing algorithms.

3. Observations of the 19 June 1992 storm

On the afternoon of 18 June 1992, a stationary front was located across northern Oklahoma. The atmospheric environment south of the front was very unstable, with a surface-based lifted index as low as -14°C. During the evening, a mesoscale convective system formed along the frontal boundary and propagated into central and southern Oklahoma. The convective part of the MCS contained tornadoes, hail, heavy precipitation, and high winds. Figure 1 shows a radar image of the convective part of the MCS at 0131 UTC 19 June. At least five significant convective cells with maximum $Z_h > 50$ dBZ are evident at the leading edge of the MCS stretching from northwest to east. As a whole, the system moved toward the southeast with an average speed of about 15–20 m s^{-1}. Rawinsonde

TABLE 1. Radar parameters.

Frequency	2735 MHz
Peak power	500 kW
Beamwidth	0.9°
Pulse width	1 μs
Receiver noise level	-110 dBm
Matched filter bandwidth	0.85 MHz
Pulse repetition frequency	814–1302 Hz
Range-gate spacing	1.0–1.6 μs
Maximum unambiguous range	115.2–184.3 km
Maximum unambiguous velocity	22.3–35.7 m s^{-1}

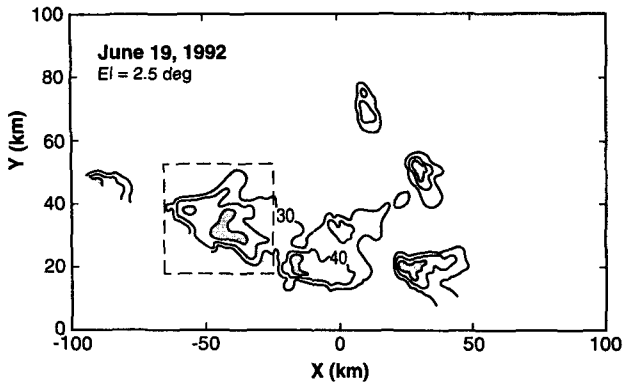

FIG. 1. Contour plot of the radar reflectivity Z_h for the squall line of 19 June 1992. In the shaded region $Z_h > 50$ dBZ. The dashed square locates the area that is analyzed in more detail.

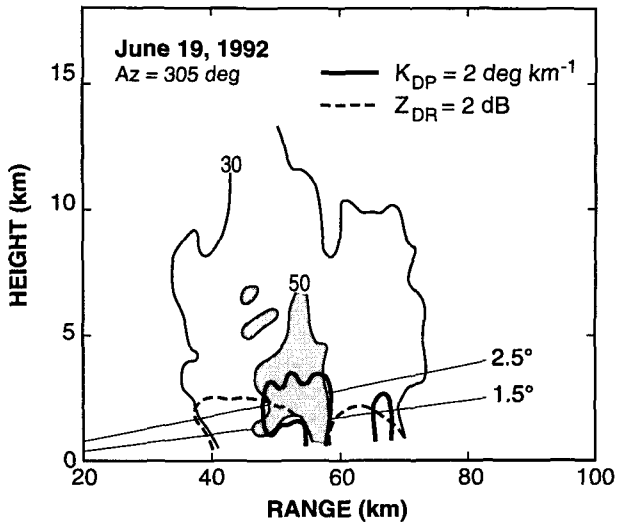

FIG. 3. Combined contour plot of Z_h, Z_{DR}, and K_{DP} in an RHI reconstructed from sector scans.

data taken at Norman (OUN) at 0000 UTC shows the freezing level (0°C) at a height of 4.1 km. Hail up to 2.5 cm in diameter was reported at 0130 UTC in the storm area. Fourteen minutes later, hailstones with diameters up to 7 cm were observed on the ground. We chose the strongest reflectivity cell in the area outlined by the square in Fig. 1 for a detailed analysis. The maximum reflectivity value reaches 58 dBZ within this region.

Figure 2 is a combined contour plot of reflectivity Z_h, differential reflectivity Z_{DR}, and specific differential phase K_{DP} in a scan at the elevation angle of 2.5°. To obtain specific differential phase K_{DP} we removed data that had signal to noise ratios less than 5 dB and averaged Φ_{DP} over 12 consecutive range locations (2.8 km). Because K_{DP} is the rate of change of Φ_{DP} with range, we estimated the slope of smoothed Φ_{DP} by averaging the increments over a 2.8-km range interval. In Fig. 2 the shaded region indicates the area with $Z_h > 50$ dBZ, the dashed line depicts a contour of $Z_{DR} = 2$ dB, and the heavy solid contour outlines the region where $K_{DP} > 2°$ km^{-1}. The 2-dB threshold for Z_{DR} is chosen to be compatible with a threshold for displaying $K_{DP} > 2°$ km^{-1} (see the appendix). In typical rain with a reflectivity factor of 50 dBZ and Z_{DR} of 2 dB, the corresponding water content is about 3 g m^{-3}, whereas K_{DP} values larger than 2° km^{-1} correspond to liquid water content of more than 2.5 g m^{-3}.

RHI (range–height indicator) of this convective cell is represented in Figs. 3 and 4 where combined plots

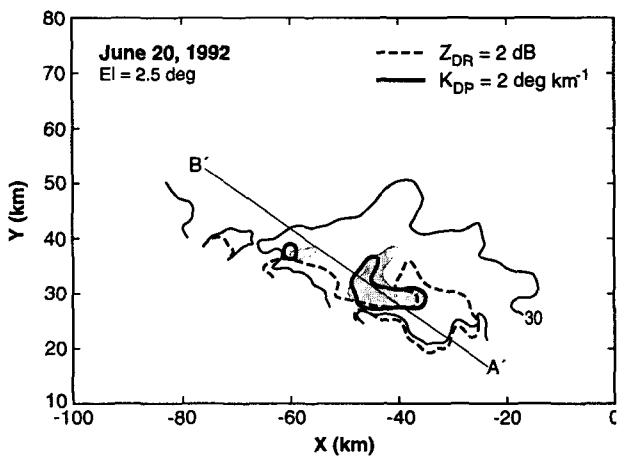

FIG. 2. Combined contour plot of Z_h, Z_{DR}, and K_{DP}. The line $A'B'$ is along the 305° azimuth; $Z_h > 50$ dBZ within the shaded area, the dashed line depicts a contour of $Z_{DR} = 2$ dB, and the heavy solid contour outlines the region where $K_{DP} > 2°$ km^{-1}. Time is 0131 UTC.

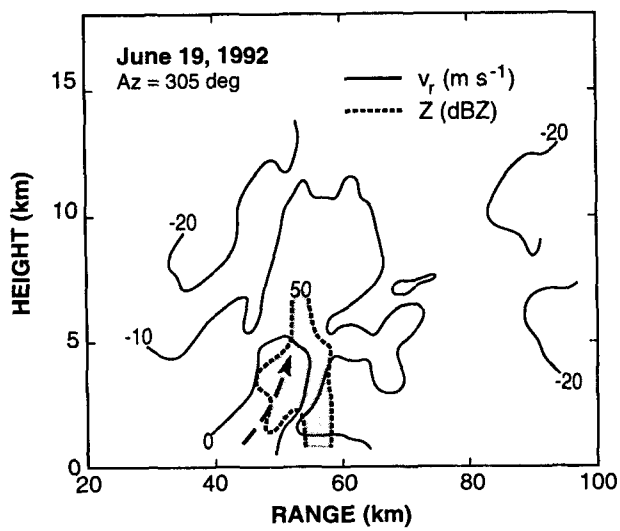

FIG. 4. Combined contour plot of Z_h and Doppler velocity in a vertical cross section (RHI). In the shaded area $Z_h > 50$ dBZ.

of Z_h together with Z_{DR} and K_{DP} (Fig. 3) or Doppler velocity v (Fig. 4) are shown. Range dependencies of Z_h, Z_{DR}, and K_{DP} can be more clearly seen by examining two radials, one pointing at 1.5°, the other at 2.5° in elevation (Fig. 5). The RHIs and radials correspond to the azimuth 305° (line $A'B'$ in Fig. 2).

A cursory look at Figs. 2–5 reveals at least four separate areas within the analyzed region that are characterized by different combinations of the observed values of radar variables. They are (a) the leading edge of updraft region (37 km $< X <$ 46 km), (b) "overhang" area (46 km $< X <$ 53 km), (c) hail-bearing main reflectivity core (53 km $< X <$ 62 km), and (d) adjacent developing cell (62 km $< X <$ 70 km). To reconcile the observed values of Z_h, Z_{DR}, and K_{DP} we assume different types of precipitation in these four areas.

a. *Leading edge of updraft region*

Very high values of differential reflectivity, up to 4.3 dB, were observed at the leading edge of the MCS at the periphery of the main reflectivity core where radar reflectivity is generally below 50 dBZ (Figs. 2, 3, and 5). At the same location K_{DP} is less than 1.0° km^{-1}. Doppler velocity measurements suggest (as indicated by the dashed arrow in Fig. 4) a strong updraft and inflow within the range interval between 40 and 50 km.

Similar observations of large Z_{DR} and moderate Z_h in precipitation from warm-based clouds have been reported by Caylor and Illingworth (1987), Meischner et al. (1991), and Bringi et al. (1991). Corresponding in situ drop size distribution measurements made on board an aircraft (Bringi et al. 1991) show an excess of large drops and a deficit of small drops with respect to the Marshall–Palmer drop size distribution (M–P DSD). This deviation from the M–P DSD is associated with the growth stage of cloud development during warm rain initiation. Bringi et al. (1991) suggest that a strong updraft plays a significant role in creating such DSDs by sorting large and small drops. The lower total concentration of raindrops diminishes the radar reflectivity, rainwater content, and K_{DP}, but at the same time, the increase of big oblate drops produces large Z_{DR}.

b. *"Overhang" area*

Distinct local maxima in Z_h and K_{DP} accompanied by large values of Z_{DR} are evident in the "overhang" area centered at 48 km (Fig. 5a). We use quotation marks to distinguish this low-level overhang from the classical overhang, which is usually located above the freezing level. In this region we could not fit estimated values of Z_{DR} and K_{DP}/Z_h to any type of DSD, assuming Pruppacher–Pitter (1971) drop shapes. Because K_{DP}/Z_h ratios were much larger than predicted for pure rain, we suspect that the dominant scatterers are liquid drops containing ice cores. These hydrometeors might have bigger dimensions and more oblateness than pure liquid raindrops (Sachidananda and Zrnić 1987). This explanation seems reasonable especially for the area with high reflectivity aloft, where the presence of small hail is likely.

c. *Hail-bearing main reflectivity core*

The main precipitation core is collocated with the downdraft, as can be seen in Fig. 4. It is apparent that the main reflectivity core (Z_h above 50 dBZ) coincides with a well-marked minimum of differential reflectivity. Figure 5 shows that the maximum of Z_h at the distance of about 55 km from the radar coincides remarkably well with the Z_{DR} minima of 1.3 dB at the elevation angle 1.5° and 0.3 dB at 2.5°. This indicates the coexistence of hail and rain. At higher elevations, the relative concentration of frozen particles is larger;

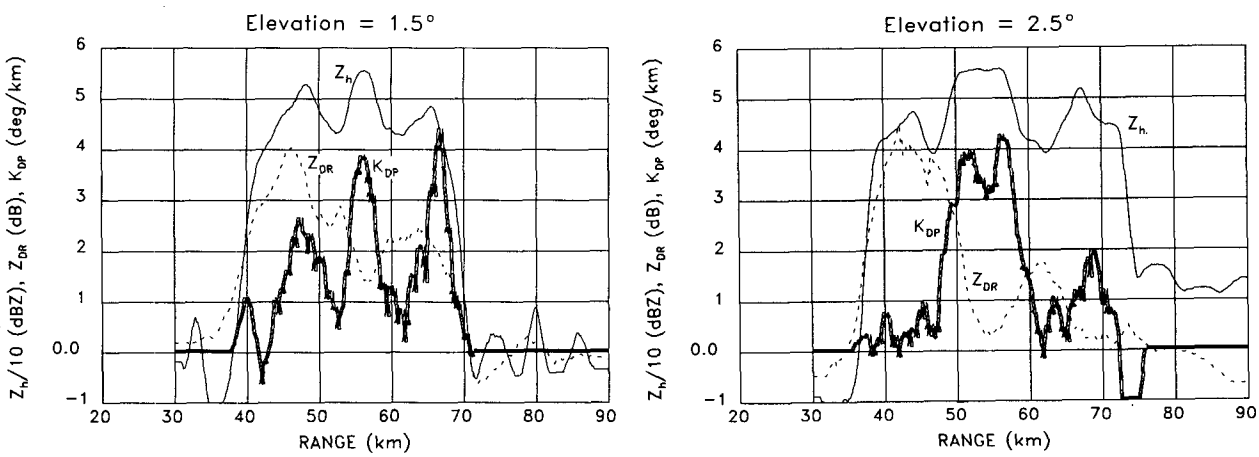

FIG. 5. Radial profiles of Z_h, Z_{DR}, and K_{DP} at the azimuth 305° for the storm of 19 June 1992.

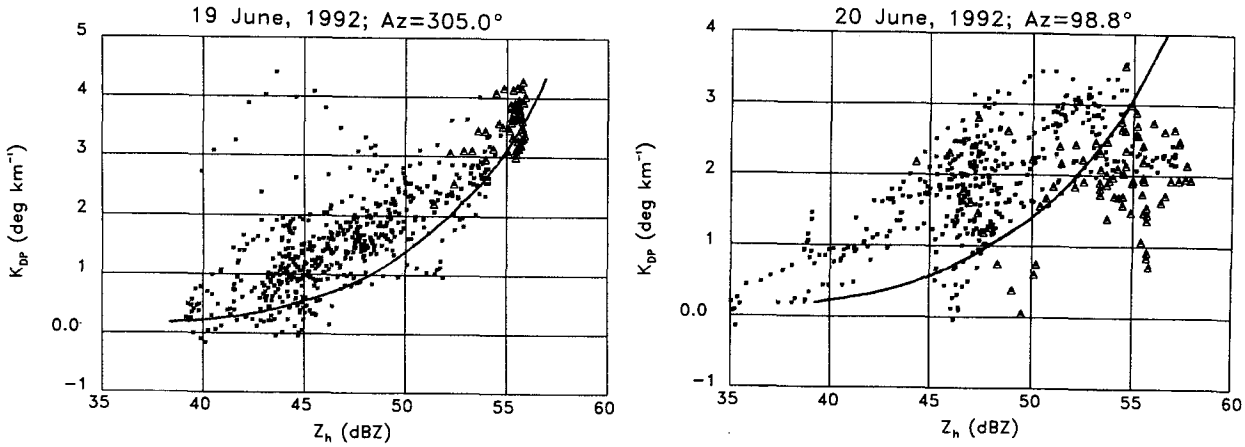

FIG. 6. Scatterplot of K_{DP} versus Z_h for the RHI data below the melting layer. Data from (a) the storm of 19 June and (b) the storm of 20 June 1992. Triangles correspond to K_{DP}, Z_h pairs in the hail-bearing region.

therefore the Z_{DR} minimum is wider and deeper for the 2.5° elevation angle.

Good correlation between Z_h and K_{DP} is evident within the main precipitation core (Figs. 2, 3, and 5), at least below the melting level. The RHI cross section (Fig. 3) shows that the $K_{DP} = 2°$ km^{-1} contour follows very well the $Z_h = 50$ dBZ contour below 3.6 km in height. There, the liquid water content could be significant (4–5 g m^{-3}) because the peak K_{DP} value is about 4° km^{-1} (see the appendix).

As already mentioned, the most plausible interpretation of the Z_h, Z_{DR}, and K_{DP} behavior within the main reflectivity core assumes the mixture of large oblate raindrops and tumbling hailstones giving comparable contributions to the radar reflectivity. Randomly oriented hailstones do not affect the specific differential phase, but significantly diminish the differential reflectivity. Well-oriented partially melted hailstones of moderate size (about 30 mm) could produce the same type of polarimetric signature (low positive Z_{DR} along with large positive K_{DP}) due to pronounced Mie effects [see Fig. 6 in Aydin and Zhao (1990)].

Another confirmation of a mixed-phase precipitation in this region is a noticeable reduction of the cross-correlation coefficient. The values of ρ_{hv} less than 0.85 were observed below the melting level between 55 and 58 km. According to Balakrishnan and Zrnić (1990b), a mixture of hydrometeors, and the distribution of sizes, shapes, and nonzero backscatter differential phase, could cause this reduction in ρ_{hv}.

d. Adjacent developing cell

This cell is centered at the range of 67 km from the radar. The peak value of Z_h (about 52 dBZ) was observed at the height of approximately 3 km above ground (Fig. 5b), whereas the peak value of K_{DP} $\approx 4°$ km^{-1} is evident at lower elevation (Fig. 5a); Z_{DR} reaches a maximum of 3.3 dB near the ground and decreases gradually with height. These observed values of radar measurands are plausible for a pure rain cell, although peak value of K_{DP} seems to be too high for the corresponding Z_h.

To examine Z_h–K_{DP} relations, we analyzed a scatterplot of Z_h and K_{DP} pairs from the RHI region below the melting level between the ranges of 40 and 70 km (Fig. 3). This scattergram is given in Fig. 6a. Triangles refer to those pairs inside the main reflectivity core with low values of differential reflectivity, that is, where mixed-phase precipitation is expected. A curve in Fig. 6a represents the Z_h–K_{DP} relation

$$Z_h = 13.86 \log(K_{DP}) + 48.2, \qquad (1)$$

which was derived for pure rain with the assumption of a Marshall–Palmer drop size distribution, and was confirmed experimentally (Balakrishnan and Zrnić 1990a). The scattergram shows that on average, for a given value of Z_h, K_{DP} is 0.5°–1.0° km^{-1} larger than predicted by (1) for pure rain. But because the triangles do not deviate substantially from the mean Z_h–K_{DP} curve we suggest that liquid precipitation is present. The apparent shift of the Z_h–K_{DP} scatterplot toward larger values of K_{DP} for moderate values of Z_h may be attributed partially to the possible negative system bias in Z_h estimate or, more likely, to the presence of ice cores in a good portion of raindrops at the altitudes 2–3 km above ground.

4. Observations of the 20 June 1992 storm

Three mesoscale convective systems developed in Oklahoma the next day. A morning system started in Kansas and moved across eastern Oklahoma, leaving an outflow boundary across north-central Oklahoma. During the afternoon, a second system formed on this boundary about 100 km north of the radar. This system

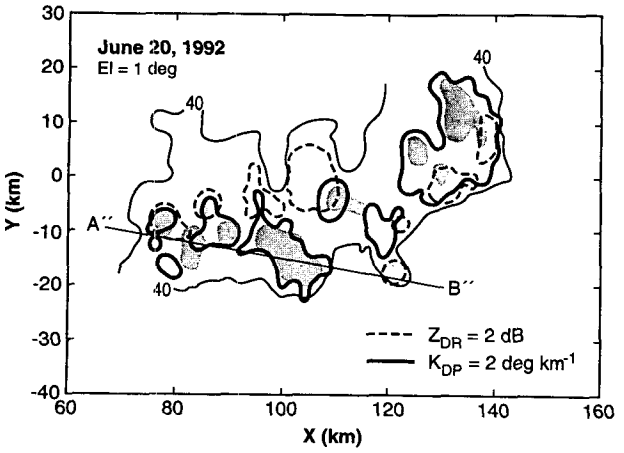

FIG. 7. Combined contour plot of Z_h, Z_{DR}, and K_{DP} for the storm at 0453 UTC 20 June 1992. The line $A''B''$ corresponds to an azimuth of 98.8°. The designation of contours is the same as in Fig. 2. Time is 0453 UTC.

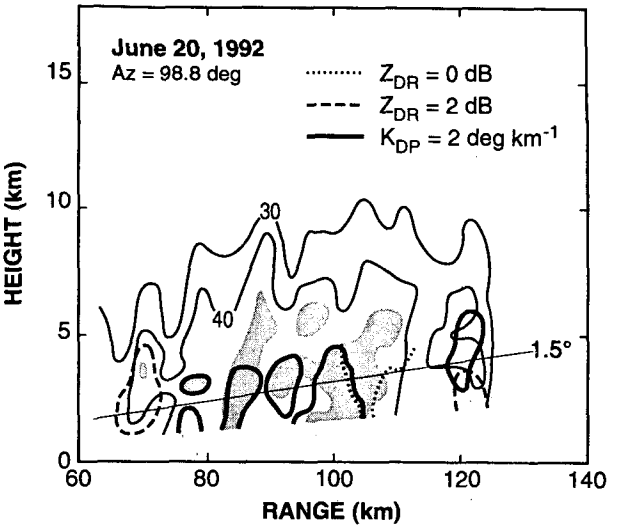

FIG. 8. Combined contour plot of Z_h, Z_{DR}, and K_{DP} in an RHI.

moved in an arc southeast to east and produced some severe weather of lesser intensity than the MCS of the previous day. A combined plot of Z_h, Z_{DR}, and K_{DP} at the elevation angle of 1.0° at 0453 UTC is shown in Fig. 7. At that time the system was moving away from the radar toward the southeast. It is evident that the main arc-shaped band extends over 70–80 km and contains several reflectivity cores that exceed 50 dBZ. Unlike the previous case (section 3), the most interesting area of the storm is now located much farther from the radar, between 70 and 140 km. Figures 8 and 9 display RHI and radial profiles of Z_h, Z_{DR}, Φ_{DP}, and ρ_{hv} at the azimuth of 98.8° along the line $A''B''$ shown in Fig. 7.

The largest convective cell centered at $X = 105$ km, $Y = -15$ km (Fig. 7) exhibits a well-defined hail signature clearly seen in Fig. 8 and especially in Fig. 9. The −1-dB minimum of Z_{DR} coincides with the peak $Z_h = 57$ dBZ at about 105 km, and is mainly caused by the abundance of hailstones; but additional Z_{DR} bias toward negative values is due to substantial differential attenuation along the propagation path through heavy precipitation in the range interval between 60 and 100 km. It can be seen from Fig. 9 that in the range interval from 100 to 115 km the differential phase Φ_{DP} deviates substantially from a monotonic curve and exhibits large spatial oscillations. We attribute these oscillations to significant backscatter differential phase δ, in the area containing hail of considerable size, as well as liquid drops. Scattering models indicate that observed $\delta \approx -40°$ (Fig. 9) could be caused by vertically elongated wet hailstones with diameters between 2 and 3 cm. This hypothesis is supported by low values of Z_{DR} (Fig. 9). A convincing argument that Mie scattering is occurring comes from the correlation signature at the distance of 105 km (Fig. 9), where ρ_{hv} drops to almost 0.4. This dip precisely coincides with the largest fluctuation of Φ_{DP}. As pointed out by Balakrishnan and Zrnić (1990b) large variations of δ within the radar resolution volume (due to the presence of non-Rayleigh scatterers such as hailstones) could significantly reduce the correlation coefficient.

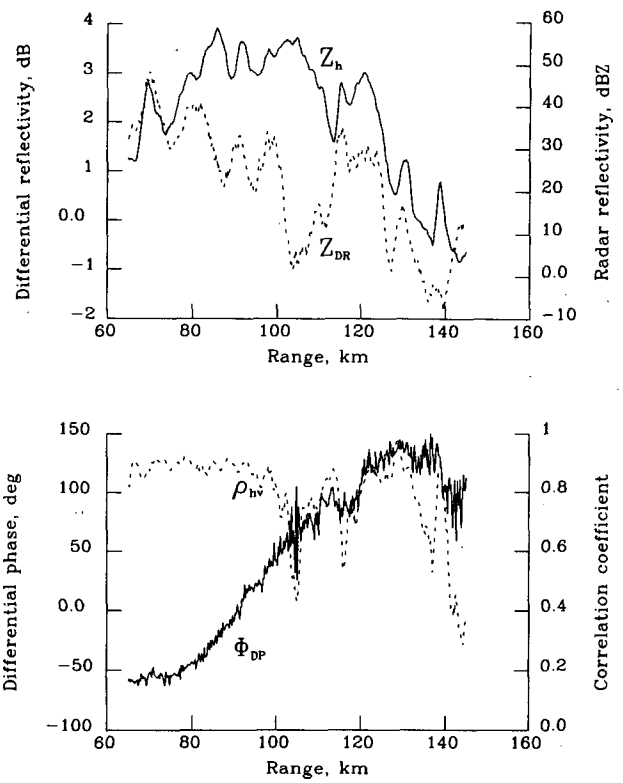

FIG. 9. Radial profiles of Z_h, Z_{DR}, Φ_{DP}, and ρ_{hv} at an elevation of 1.5° and azimuth of 98.8° for the storm of 20 June 1992.

Other convective cells in the squall line do not bear significant amounts of hail and produce liquid precipitation. The only exception is the cell centered at 85 km with a reflectivity peak of 57 dBZ accompanied by local minimum in Z_{DR} (Fig. 9); Φ_{DP} and ρ_{hv} range dependencies in this area do not show significant contribution from backscatter differential phase and the peak value of K_{DP} is about 2.5° km^{-1} there. This means that the contribution of hail to the radar signal is less here than in the largest reflectivity cell.

Enhanced values of Z_{DR} observed in the cells at 65 and 120 km can be attributed possibly to a growth stage of development like in the case of 19 June.

Because the storm of 20 June extended over a wide area and contained very high amounts of liquid water, we observed tremendous differential phase signatures within the radar echo area. Differential phase Φ_{DP} increases over 200° along the propagation path through the precipitation region. For the first time during our observations we encountered aliasing because Φ_{DP} is unambiguous within a 180° interval.

Specific differential phase K_{DP} generally is well correlated with Z_h (see Figs. 7–9). As in the case of 19 June, observed values of K_{DP} seem to be higher for corresponding values of Z_h than predicted by theory. We have examined K_{DP}, Z_h scattergram for the radials at elevations 1.0° and 1.5° (Fig. 6b). The triangles in the scattergram correspond to the hail-bearing zone ($Z_{DR} < 1$ dB and $Z_h > 50$ dBZ). In contrast to the scattergram of 19 June (Fig. 6a), the triangles are dispersed over an extended area in the Z_h–K_{DP} plane. That is because the contribution of the backscatter differential phase is significant. As mentioned earlier, an apparent shift toward larger K_{DP} in the scattergram is possibly caused by the presence of ice cores inside liquid hydrometeors.

5. Differential attenuation analysis

Because attenuation by rain at a 10-cm wavelength is small there is a widespread belief that specific differential attenuation A_{DP} (i.e., the difference in specific attenuation between horizontally and vertically polarized waves propagating through precipitation) is negligibly small. Our experience suggests that this is not true, at least in the case of Oklahoma storms. As can be seen from Fig. 9, the differential reflectivity gradually decreases in the mean with increasing range. At the far side of storms, negative values of Z_{DR} are frequently observed in areas behind extended zones of large reflectivity. Negative Z_{DR} bias can be as large as 1–2 dB. Consequently, Z_{DR} data should be corrected for differential attenuation in severe storms. Differential reflectivity bias ΔZ_{DR}, due to differential attenuation, can be expressed as:

$$\Delta Z_{DR}(R) = 2\int_0^R A_{DP}(r)dr, \qquad (2)$$

where R is range from the radar. It is not easy to estimate A_{DP} from radar data for each point along a propagation path, but it is possible to evaluate the whole integral on the right side of (2) using measurements of differential phase shift Φ_{DP} as suggested by Bringi et al. (1990). These authors assumed that a linear relationship, $A_{DP} = cK_{DP}$, between specific differential attenuation and specific differential phase is valid for liquid precipitation. Because total differential phase (neglecting the contribution of backscatter differential phase) is an integral of K_{DP} over the same propagation path, we can directly estimate $\Delta Z_{DR}(R)$ using $\Phi_{DP}(R)$ measurements:

$$\Delta Z_{DR} = c\Phi_{DP}. \qquad (3)$$

Strictly speaking, A_{DP} is not linearly dependent on K_{DP}; furthermore, the relation between them is not unique, due to DSD variations and temperature influence. Jameson (1992) suggested a power relation, $A_{DP} = cK_{DP}^b$, where the coefficient c depends on temperature. Nevertheless, according to Jameson (1992), at a 10-cm wavelength the nonlinearity is very weak (b is about 1.05) and therefore, (3) should be approximately valid.

There is no doubt that the rate of Z_{DR} decrease with range is in close agreement with the rate of Φ_{DP} increase. Figure 10 confirms this statement. For the radial at 98.6° we see an extraordinary decrease of Z_{DR} with distance, which coincides with a fast increase of Φ_{DP} (solid line); this is in contrast to the rather "plain" profiles of these two quantities for the radial at 83.8° (dashed lines). Next, we describe an attempt to quan-

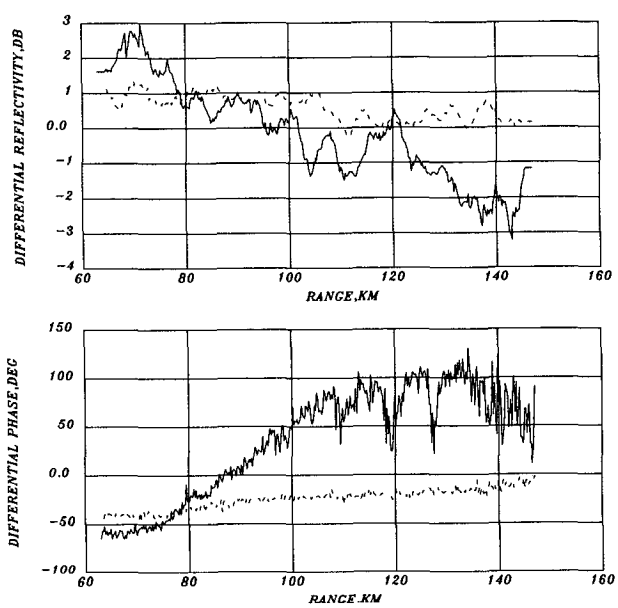

FIG. 10. Radial profiles of (a) Z_{DR} and (b) Φ_{DP} at the elevation of 2.0° and azimuth of 98.6° (solid line) and 83.8° (dashed line) for the storm on 20 June.

titatively evaluate this interrelation, that is, to empirically estimate the coefficient of proportionality c in (3). We examined Z_{DR}, Φ_{DP} scattergrams using data from several radials at an elevation angle of 1.0° for the storm of 20 June. The low elevation angle was chosen to reduce the influence of height on Z_{DR}, and to insure that there is no contribution from the melting layer. Furthermore, only data with reflectivity factors smaller than 40 dBZ are plotted (Fig. 11) to avoid contamination by hail.

The estimated slope $c = 0.0083$ (Fig. 12) is considerably larger than the theoretically predicted values (Bringi et al. 1990; Jameson 1992). One possible explanation of this discrepancy is the following. For monodispersed oblate raindrops with equilibrium shape the A_{DP}/K_{DP} ratio (or the coefficient c) heavily depends on equivolume drop diameter (Fig. 12, thin solid curve). Calculations were made using standard T-matrix technique at the temperature of 15°C. The long-dashed line corresponds to the predicted A_{DP}/K_{DP} ratio given by Bringi et al. (1990) for $T = 15$°C. The short-dashed lines depict the interval to which this ratio belongs in the temperature range between 0° and 20°C according to Jameson (1992). Obviously the single drop relations and the two theories produce essentially equivalent results for drops up to about 5 mm in diameter. The double solid line represents our empirical estimate from the scatterplot in Fig. 11. The coefficient c is largest if very big drops are present in the drop size distribution. Thus, it appears that in observed storms, the DSD contained more drops with larger diameters than those simulated in theoretical studies, or large drops were more oblate than the equilibrium drops. As pointed out by Sachidananda and Zrnić (1987), large hydrometeors in Oklahoma may be partially melted ice, which have minor to major axis ratios smaller than pure liquid drops. This conclusion is consistent with the K_{DP}–Z_h scattergrams (Fig. 6), which show a K_{DP} shift toward larger positive values with respect to prediction for pure rain.

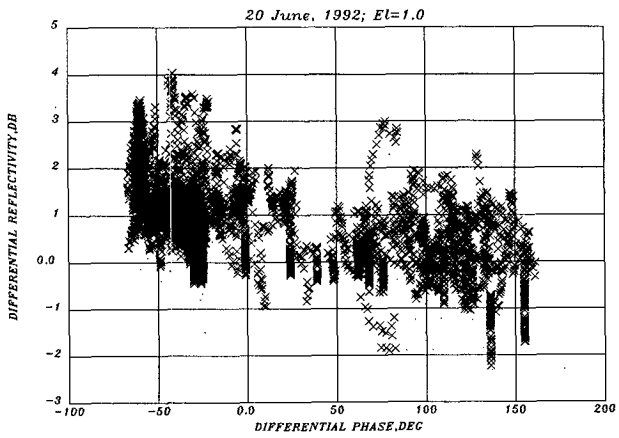

FIG. 11. Scattergram of Z_{DR} versus Φ_{DP} for range gates below the melting level.

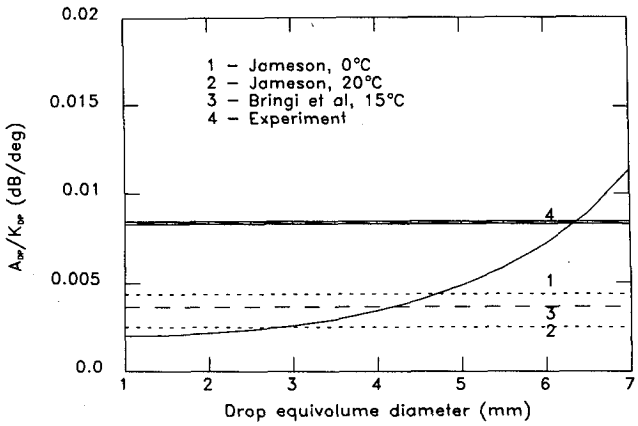

FIG. 12. The dependence of A_{DP}/K_{DP} ratio on drop diameter for monodispersed liquid precipitation at S band (thin solid line). The results of theoretical computations and experimental estimate for polydispersed precipitation are shown as reference levels.

The MCS of 20 June caused a significant attenuation of the propagating waves. We can estimate a lower bound for the total attenuation using the formula from Bringi et al. (1990) that relates Φ_{DP} and total attenuation loss L (dB). For the observed maximum $\Phi_{DP} = 200°$, we obtain $L = 3.3$ dB. This is a conservative estimate, because the relationship assumes equilibrium drop shapes. But a significant number of drops along the propagation path were more oblate and larger than typical rain. Consequently, as with differential attenuation, the cumulative attenuation could be larger by as much as a factor of 2.

6. Conclusions

Recent upgrades of the Cimarron polarimetric radar provide us with unique opportunities to obtain fields of three polarimetric variables, Z_{DR}, Φ_{DP}, and ρ_{hv}, along with Z_h, in real time; thus their joint analysis becomes possible over extended spatial volumes. We have examined two Oklahoma mesoscale convective systems containing heavy precipitation, and were able to get interpretable polarimetric information up to 140 km from the radar.

The analysis of the whole set of polarimetric variables reveals at least three types of hydrometeor populations in convective cells within these MCSs. One seems to be characterized by large positive values of Z_{DR} (3–4 dB), and K_{DP} smaller than 1° km^{-1} below the melting layer; this has been observed in the growth stage, and the corresponding hydrometeors could be mainly large raindrops. The other set of hydrometeors produces basically the same Z_{DR} values (3–4 dB), and K_{DP} values between 1° and 2.5° km^{-1}; it is also associated with the growth stage, and our analysis suggests that a good portion of the hydrometeors are large oblate drops

containing ice cores. The third clearly discernible population consists of hail with and without rain; for this population of hydrometeors, Z_{DR} is close to zero, while ρ_{hv} can drop below 0.75–0.85. Specific differential phase K_{DP} is usually high in these zones and sometimes pronounced differential phase shift upon scattering is evident, which we attribute to large wet hailstones (main core in the storm of 20 June). In one such cell, extremely low values of cross-correlation coefficient (as low as 0.4) were found.

We have made an attempt to quantify the amount of liquid water using the polarimetric variables. Simple formulas for estimating rainwater were often inconsistent and thus not applicable because precipitation particles were not drops with equilibrium shapes. Nevertheless, experimental data suggest that the differential phase shift Φ_{DP}, and its derivative K_{DP}, are reliable indicators of liquid water in heavy precipitation. We have encountered a cumulative differential phase of 200° within the 20 June storm.

A negative bias of Z_{DR}, due to differential attenuation in precipitation, could be significant for these types of storms, and therefore must be accounted for. A suitable correction scheme uses Φ_{DP} measurements and a relation between A_{DP} and K_{DP}. Experimental evaluation of the ratio A_{DP}/K_{DP} indicates that it was underestimated at least twofold in the previous theoretical predictions. Consequently, actual Z_{DR} biases appear to be much larger than expected. To explain this discrepancy, we hypothesize that the largest drops originated from melting hailstones and contained ice cores. Such hydrometeors can have larger diameters and can be more oblate than typical raindrops. This argument also explains some experimentally observed values of K_{DP}, which are larger than those predicted from model considerations of pure rain.

We conclude that the described polarimetric datasets are consistent with theoretical expectations. Furthermore, these data demonstrate the potential utility of radar polarimetry for determining precipitation type in severe storms and discriminating between rain and hail.

Acknowledgments. D. Sirmans and J. Carter have contributed substantially to the installation of the polarization switch and changes in the antenna assembly. A. Zahrai designed and implemented the upgrade of the Cimarron radar. M. Schmidt has made numerous design changes and modifications of various hardware; he is also maintaining the facility with the help of G. Anderson and R. Wahkinney. A. Witt and N. Balakrishnan gave valuable criticisms of the manuscript. Yosepha Gal-Chen assisted us in various aspects of data manipulations. Joan O'Bannon prepared graphics.

APPENDIX

Relations between Liquid Water Content and Polarimetric Variables

The relations between the liquid water content M and the polarimetric variables are presented here. These relations also justify our choice of several thresholds in the display of the radar data. There are no published equations relating M with Z_h and Z_v, hence we derived one based on the procedure of Sachidananda and Zrnić (1987), who varied the exponent Λ and the concentration N_0 of exponential drop size distribution. The relation is

$$M = 1.06 \times 10^{-3} Z_h^{0.86} \left(\frac{Z_v}{Z_h}\right)^{4.18}, \quad \text{(A1)}$$

where $Z_{h,v}$ are reflectivity factors ($mm^6\ m^{-3}$) for horizontal and vertical polarization and M is in grams per cubic meter. A similar relation was obtained by V. Chandrasekar (1992, personal communication), who varied the parameters of a gamma drop size distribution. The relation is

$$M = 1.13 \times 10^{-3} Z_h^{0.89} \left(\frac{Z_v}{Z_h}\right)^{4.62}. \quad \text{(A2)}$$

The same procedure and sources made the following two relations available:
Sachidananda and Zrnić (1987):

$$M = 1.63 K_{DP}^{0.76}; \quad \text{(A3)}$$

Chandrasekar (1992, personal communication):

$$M = 1.36 K_{DP}^{0.87}, \quad \text{(A4)}$$

where K_{DP} is in degrees per kilometer.

Finally, a relation between M, Z, and Λ can be derived from an assumed exponential drop size distribution:

$$M = \frac{10^{-3} Z \Lambda^3 \pi}{720}. \quad \text{(A5)}$$

Next we demonstrate that the threshold values of 2° km^{-1} for K_{DP}, 50 dBZ for Z_h, and 2 dB for Z_{DR} are compatible. Equations (A3) and (A4) yield M of 2.8 and 2.5 g m^{-3}. If we assume a Marshall–Palmer relation between rain rate R and Λ, $\Lambda = 4.1 R^{-0.21}$, $Z = 50$ dBZ, and $Z = 200 R^{1.6}$, and then substitute these in (A5), we obtain $M = 2.6$ g m^{-3}. Thus the K_{DP} and Z_h thresholds are compatible. It can be shown that at $Z_h = 50$ dBZ, the Z_{DR} threshold of 2 dB corresponds to somewhat larger liquid water contents of 3 g m^{-3} for (A1) and 3.7 g m^{-3} for (A2). But examination of the sensitivity to changes in Z_h/Z_v reveals that (A1) and (A2) would produce values of M of 2.5–2.6 g m^{-3} if the differential reflectivity is 2.2–2.3 dB. Thus, 2 dB is a compatible rounded off value that is easy to remember and convenient to use.

REFERENCES

Aydin, K., and Y. Zhao, 1990: Computational study of polarimetric radar observables in hail. *IEEE Trans. Geosci. Rem. Sens.*, **28**, 412–422.

——, Giridhar, and Y. Zhao, 1991: Polarimetric C-band radar observables in melting hail: A computational study. Preprints, *25th Conf. on Radar Meteorology,* Paris, Amer. Meteor. Soc., 733–736.

Balakrishnan, N., and D. S. Zrnić, 1990a: Estimation of rain and hail rates in mixed phase precipitation. *J. Atmos. Sci.,* **47,** 565–583.

——, and ——, 1990b: Use of polarization to characterize precipitation and discriminate large hail. *J. Atmos. Sci.,* **47,** 1525–1540.

Bringi, V. N., V. Chandrasekar, N. Balakrishnan, and D. S. Zrnic, 1990: An examination of propagation effects in rainfall on radar measurements at microwave frequencies. *J. Atmos. Oceanic Technol.,* **7,** 829–840.

——, D. A. Burrows, and S. M. Menon, 1991: Multiparameter radar and aircraft study of raindrop spectral evolution in warm-based clouds. *J. Appl. Meteor.,* **30,** 853–880.

Carter, J. K., D. Sirmans, and J. Schmidt, 1986: Engineering description of the NSSL dual linear polarization Doppler weather radar. Preprints, *23rd Conf. on Radar Meteorology,* Snowmass, CO, Amer. Meteor. Soc., JP381–JP384.

Caylor, I. J., and A. J. Illingworth, 1987: Radar observations and modelling of warm rain initiation. *Quart. J. Roy. Meteor. Soc.,* **113,** 1171–1191.

Illingworth, A. J., and I. J. Caylor, 1989: Cross polar observation of the bright band. Preprints, *24th Conf. on Radar Meteorology,* Tallahassee, Amer. Meteor. Soc., 323–327.

Jameson, A. R., 1992: The effect of temperature on attenuation-correction schemes in rain using polarization propagation differential phase shift. *J. Appl. Meteor.,* **31,** 1106–1118.

Leitao, M. J., and P. A. Watson, 1984: Application of dual linearly polarized radar data to prediction of microwave path attenuation at 10–30 GHz. *Radio Sci.,* **19,** 209–221.

Meischner, P. F., V. N. Bringi, D. Heimann, and H. Holler, 1991: A squall line in southern Germany: Kinematics and precipitation formation as deduced by advanced polarimetric and Doppler radar measurements. *Mon. Wea. Rev.,* **119,** 678–701.

Pruppacher, H. R., and R. L. Pitter, 1971: A semi-empirical determination of the shape of cloud and rain drops. *J. Atmos. Sci.,* **28,** 86–94.

Sachidananda, M., and D. S. Zrnić, 1987: Rain rate estimated from differential polarization measurements. *J. Atmos. Oceanic Technol.,* **4,** 588–598.

Zahrai, A., and D. S. Zrnic, 1993: The 10-cm wavelength polarimetric weather radar at NOAA's National Severe Storms Laboratory, *J. Atmos. Oceanic Technol.,* **10,** 649–662.